Anisotropic shape of self-assembled InAs quantum dots: Refraction effect on spot shape of reflection high-energy electron diffraction

Takashi Hanada, Bon-Heun Koo, Hirofumi Totsuka, and Takafumi Yao
Institute for Materials Research, Tohoku University, Sendai 980-8577, Japan
(Received 26 March 2001; published 3 October 2001)

A significant role of refraction effect on reflection high-energy electron diffraction (RHEED) from nanostructures is demonstrated. It was found that the chevron-shape spots in RHEED patterns from self-assembled InAs/GaAs(001) and InAs/InAlAs/InP(001) quantum dots at $[1\bar{1}0]$ azimuth are well reproduced by kinematical calculations taking into account the refraction of electron beam at the curved surfaces of the dots. The dots must have $(1\bar{1}0)$ cross sections steeper than (110) cross sections and consequently extend along $[1\bar{1}0]$ since the refraction effects, considerable only at glancing incidence and departure, are invisible at [110] azimuth.

DOI: 10.1103/PhysRevB.64.165307 PACS number(s): 61.14.Hg, 68.55.Jk, 68.65.−k, 81.15.Hi

I. INTRODUCTION

Recently, nature and growth techniques of the strain-induced quantum dot structures are actively studied from the viewpoints of fundamental physics as well as device applications. In order to understand the growth process of the dots, knowledge about the shape of the as-grown dots is particularly important. Furthermore, detailed electronic structure of dot, which governs electronic and optical properties such as polarization anisotropy, depends on the shape.[1–3]

One of the informations about the dot shape has been provided by reflection high-energy electron diffraction (RHEED); It is well known that the chevron-shape spots appear in RHEED patterns from self-assembled InAs/GaAs(001) quantum dots at $[1\bar{1}0]$ azimuth while ordinary oval spots are observed at [110] azimuth.[4–6] At first, the chevron was attributed to reciprocal rod normal to (113) and $(\bar{1}\bar{1}3)$ facets because the angle between the two chevron-tails is about 55°.[4] However, the fact that chevron-tails always appear in the low take-off angle side of the diffraction spots irrespective of the spot indices and glancing and azimuthal angles around $[1\bar{1}0]$ cannot be explained well by the facet originated streaks. Later, {136} facets which have the same $(1\bar{1}0)$ cross section with {113} facet was proposed based on the observation of facetlike streaks in the high take-off angle side at $[3\bar{1}0]$ azimuth.[1,6,7] However, clear mechanism about the appearance of the widely-observed chevron spots at $[1\bar{1}0]$ has not been given for the {136}-facet dots. Similar chevron spots are also observed from InAs/InAlAs/InP(001) dot system with smaller 3% lattice misfit, where the angle between the tails is about 40°, which attributed to {114} facets.[8] However, the cross sectional image of the dot observed by transmission electron microscope (TEM) shows that the tilt angle of the facet is different from the half of the angle between the chevron tails.

So far, importance of the refraction effect on the electron diffraction from nanostructures has not been recognized widely. In the present study, we will propose an interpretation that refraction at the dot surface induces the chevron spots whose tails always appear in the lower takeoff angle side. This mechanism requires the dots to have curved surfaces at least at the $[1\bar{1}0]$ and $[\bar{1}10]$ azimuths for the continuous variation of the refraction direction. Furthermore, the angle between the chevron tails mainly depends on the height vs base diameter ratio of the domelike dots.

II. EXPERIMENT

The experiments were carried out in a MBE chamber equipped with a RHEED apparatus. The growth procedures of InAs dots on GaAs(001) and on $In_{0.52}Al_{0.48}As$ lattice matched to InP(001) are described in Refs. 9 and 10, respectively. After the native oxide layer was thermally removed in As_4 ambient, a 300 nm thick GaAs buffer layer was grown on GaAs at 840 K and a 500 nm thick InAlAs buffer layer was grown on InP at 800 K. InAs was deposited at 750 K at a growth rate of 0.07 monolayer/s (ML/s) on the GaAs buffer layer and at 780 K and 0.3 ML/s on the InAlAs buffer layer, where 1 ML is 6.26×10^{14} InAs molecules/cm^2. RHEED pattern was observed *in situ* during the growth. The kinetic energy of the electron beam was 20 keV. Atomic force microscope (AFM) observations were carried out in air at room temperature.

III. RESULTS AND DISCUSSION

Typical RHEED patterns of the InAs dots grown on GaAs(001) and on InAlAs/InP(001) at [110] and $[1\bar{1}0]$ incident azimuths are shown in Fig. 1. The shadow edge, which corresponds to the line of zero take-off angle from the substrate surface, is located around the bottom of each pattern. It is obvious that the dots have an anisotropic structure because the chevron spots appear only at $[1\bar{1}0]$ azimuth while spots at [110] have oval shape. The angle between the chevron tails from InAs/GaAs dots [Fig. 1(b)] is larger than that from InAs/InAlAs/InP dots [Fig. 1(d)] in agreement with previous observations.[4–6,8]

Kinematical calculations of RHEED patterns from an InAs dot, 1 ML InAs wetting layer, and semi-infinite GaAs(001) substrate system were carried out. The atomic structure of the system was relaxed by minimizing the Stillinger-Weber strain energy.[11,12] In Fig. 2(a), a relaxed

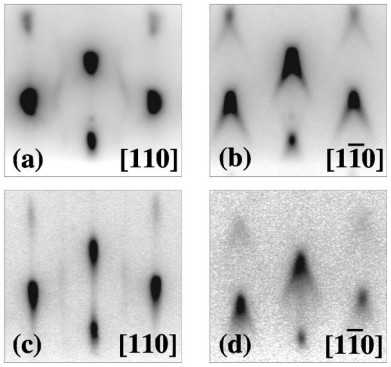

FIG. 1. Typical RHEED patterns of InAs quantum dots on GaAs(001) {(a) and (b)} and on InAlAs/InP(001) {(c) and (d)} observed at [110] and [1$\bar{1}$0] azimuths.

atomic structure of a domelike dot (base diameter is 17 nm) is shown along the (1$\bar{1}$0) cross section illustrated by hatching in the inset, where the center and the area of each circle indicate the position and the partial strain energy of the corresponding atom. The partial strain energy of each atom is defined as the summation of half of the energy produced by the bond-length modifications of the four bonds around the atom and all of the energy produced by the bond-angle modifications of the six bond pairs around the atom. Surface reconstruction was ignored and surface dangling bonds were not taken into account. Therefore, the strain energy of a surface atom is small not only due to freedom in outward displacement but also due to reduction of the number of bonds. A periodic boundary condition of a square in-plane superlattice, whose boundary of the wetting layer and the substrate is the same as shown in Fig. 2(a), was assumed and the substrate layers below the layers shown in Fig. 2(a) were fixed at their bulk positions. Around the InAs/GaAs interface, atoms at the center of the dot move upward and atoms at the edge of the dot move downward as shown in Fig. 2(b), i.e., the interface bends to reduce the misfit strain of the uncapped dot since there is a free space above the dot. The height difference between the highest (center) and lowest (edge) atoms in the base In layer is about 0.5 Å. Figure 2(c) displays local hydrostatic strain distribution around each cation atom calculated from the relaxed atomic coordinates using the method of Ref. 13. The substrate atoms below the center of the dot are under tensile strain due to the bending while those around the edge of dot are under compressive strain. This strain distribution around an uncapped dot is in contrast with the compressive hydrostatic strain of the substrate atoms just below the center of an InAs dot capped by a GaAs layer.[1,13]

The atomic scattering factors of electron calculated by Doyle and Turner[14] were used in the kinematical calculations. Debye-Waller factors were evaluated assuming isotropic rms thermal vibrational amplitude of 0.2 Å for all atoms. Attenuation of the electron beam is taken into account by considering total number of atoms per area above a scattering atom.[9] Therefore, the absorption coefficient of the electron beam in the dot layer is proportional to the dot density and scattering from the two-dimensional (2D) layers

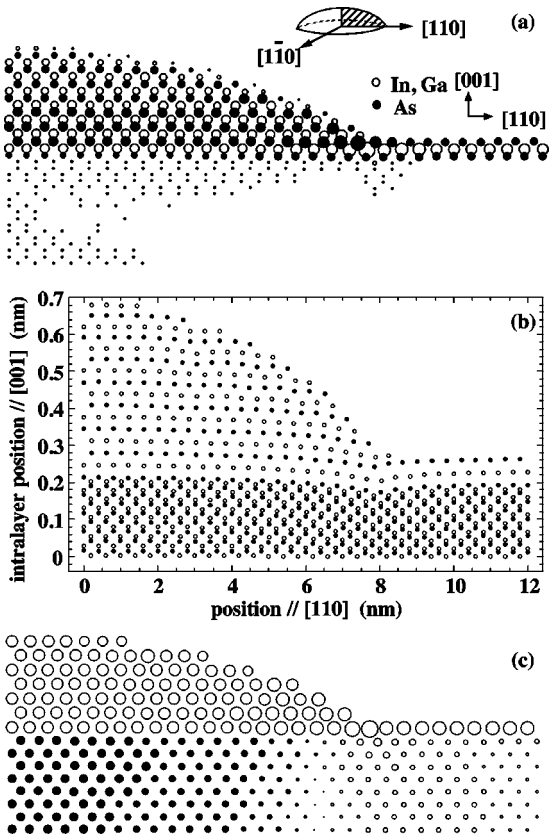

FIG. 2. (1$\bar{1}$0) cross section of the relaxed atomic structure of a domelike InAs dot (base diameter 17 nm), 1 ML wetting layer, and GaAs(001) substrate. (a) Center and area of each circle indicate the position and partial strain energy of the corresponding atom, respectively. (b) Map of atomic positions where interlayer distances between neighboring layers shrink by 1.3 Å and the vertical scale is ten times larger than the horizontal one to display the vertical displacements clearly. (c) Area of each circle indicates local hydrostatic strain of the corresponding cation atom surrounded by four As atoms. Open and closed circles represent compressive and tensile strain, respectively.

have little influence on the pattern when net coverage of the dots smoothed to be 2D layer exceeds about 1 ML, i.e. the total volume of the dots is equivalent to 1 ML of deposited material. All patterns shown here are calculated for the dot coverage of 1 ML at glancing angle 1° to the substrate.

Figures 3(a) and 3(b), respectively, show calculated patterns at [1$\bar{1}$0] azimuth for a {113}-facet dot and a {114}-facet dot, whose base length is 16 nm. Similar patterns are also obtained at [110] because the dots have isotropic shapes. In Fig. 3, the bottom line of each pattern corresponds to the shadow edge and the weak 10% intensity levels occupy 90% of the gray scale levels to enhance the weak structures. It must be noted that the strong reflections in the observed patterns are also saturated. There are faint oblique streaks, whose direction is nearly perpendicular to the corresponding facet.[15] However, the observed characteristic shape of the chevron is not reproduced by the facet-originating streaks.

On the other hand, it has been observed that refraction of the electron beam at surface causes some shifts of the Bragg

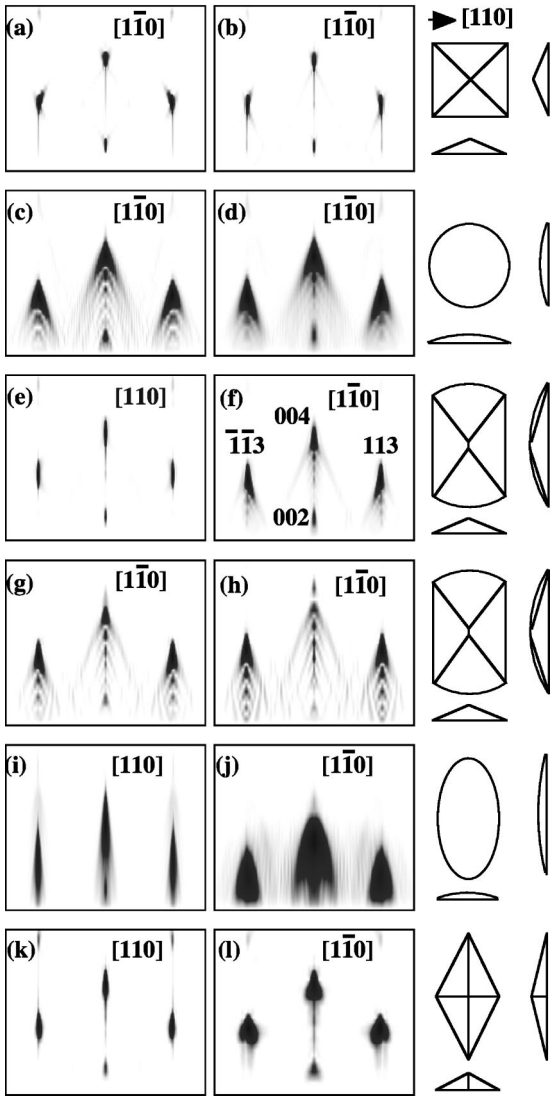

FIG. 3. Calculated RHEED patterns of InAs {except (g) of $In_{0.5}Ga_{0.5}As$ and (h) of GaAs} quantum dots grown on GaAs(001) for several shapes at $[110]$ and $[1\bar{1}0]$ azimuths: (a) {113}-facet dot; (b) {114}-facet dot; (c) and (d) domelike dot; (e), (f), (g), and (h) domelike dot truncated by (114) and $(\bar{1}\bar{1}4)$ facets; (i) and (j) domelike dot elongated along $[1\bar{1}0]$; (k) and (l) {136}-facet dot. Schematic top and side views of each dot are shown on the right side of the corresponding pattern.

reflection peaks in a RHEED rocking curve and that the shift increases up to about 1° with decreasing glancing angle to 0°.[16] Since the dot surface is not parallel to the substrate surface, the glancing angle of the electron beam to the dot surface is generally position dependent. Therefore, it is possible that the refraction causes serious modifications in a RHEED pattern.

The electron beam, whose wave number is k_v in vacuum, is accelerated in a solid with positive mean inner potential U_0, which is 15 eV for InAs evaluated from the atomic scattering factors[14] and volume density of atoms. As a result, the wave number inside the solid becomes $k_s = \sqrt{k_v^2 + 2m\hbar^{-2}U_0}$ and the beam is refracted to conserve the

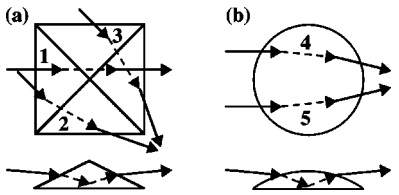

FIG. 4. Schematic top and side views of electron beam refractions at facet (a) and domelike (b) surfaces and scatterings in the dots.

surface-parallel component of the wave vector. The wave vector $\mathbf{k}_s$ inside the solid is given by

$$\mathbf{k}_s = \mathbf{k}_v + (\sqrt{(\mathbf{k}_v \cdot \mathbf{n}_{\mp})^2 + 2m\hbar^{-2}U_0} - \mathbf{k}_v \cdot \mathbf{n}_{\mp})\mathbf{n}_{\mp}, \quad (1)$$

where $\mathbf{k}_v$ is the wave vector in vacuum, $\mathbf{n}_{\mp}$ is the normal vector of the surface (toward solid for an incident beam and toward vacuum for an outgoing beam) at the point of incidence or exit. First, the points of incidence and exit are calculated from the position of each scattering atom, and then wave vectors inside and scattering angle at the atom are calculated for the given incident and out-going wave vectors in vacuum.

Figure 3(c) shows a pattern calculated with the refraction effect for a domelike (part of sphere) dot, whose base diameter d is 16 nm and height h is 2 nm. In spite of the absence of any facets, the spots have chevron shapes which agree well with the observed ones except for the weak fringes below the chevron tails. These fringes are due to a size effect and the distance between the fringes become narrow with increasing dot size just like the Laue fringes of thin-film x-ray diffraction. In the superposed pattern of Fig. 3(d) with various d from 8 to 16 nm at the same h/d ratio, the fringes become less visible. The calculated chevron tails of the domelike dot have much stronger intensity than the facet-originating streaks surveyed by the gray scale change. Moreover, it was confirmed that the tails disappeared, if the refractions were not included in the calculations.

The appearance of the tails due to the refractions at a curved surface can be understood as follows. At the incident and exit points on the dot surface, the electron beam is refracted in a manner attracted into solid (the side views in Fig. 4) as Eq. (1). As a result, the scattering angle observed in the vacuum is always smaller than that in the solid and the position of a Bragg spot observed in the vacuum always shifts to lower takeoff angle side although the shift depends on the surface normal vectors at the entrance and exit of the electron beam. When the normal vector at the dot surface is out of the incident plane of the beam to the substrate (e.g., path 2, 3, 4, and 5 in Fig. 4), the substrate-parallel direction of the electron beam is also shifted and the refracted beam is shunted to the oblique chevron tail direction. In addition, since the normal vector of the domelike dot surface inclines continuously from the top to the base, the refracted beam direction has a continuous distribution to form the long chevron tail. The wave length of 20 keV electron is about 0.087 Å and the envelope surface of dot looks flat enough in this scale to define the direction of refraction at a certain point. Therefore, as shown in Fig. 3(d), it is most probable

that the chevron spots are originated from the refractions of electron beams at the incident and exit points on a curved surface.[17] In this model, the angle between the chevron tails depends on the steepness of the dome (h/d ratio); the angle becomes large when the dome becomes steep.

In the calculations of Figs. 3(a) and 3(b), the refraction effect was also included. However, since the $(1\bar{1}3)$ and $(1\bar{1}4)$ facets incline about 25° and 20°, respectively, from the (001) substrate, the shift of the beam direction at $[1\bar{1}0]$ incidence is only about 0.05° normal to the substrate (path 1 in Fig. 4) and consequently no refraction-induced oblique tails appears in this case. Here, separation between the neighboring integer-order reciprocal rods at $[1\bar{1}0]$ azimuth is 1.24° at 20 keV. Furthermore, incident flux density to $(11n)$ and $(\bar{1}\bar{1}n)$ side facets is negligible at the $[1\bar{1}0]$ incident azimuth because of a small glancing angle of RHEED.

The isotropic domelike dot, however, disagrees with the anisotropy of the RHEED pattern shown in Fig. 1; Similar chevron pattern appears also at [110] azimuth. When a dot has domelike surface at the $[1\bar{1}0]$ and $[\bar{1}10]$ azimuths and steeper single or a few facets facing the [110] and $[\bar{1}\bar{1}0]$ azimuths, the refractions are less effective at [110] azimuth. Figures 3(e) and 3(f) show calculated RHEED patterns at [110] and $[1\bar{1}0]$ azimuths, respectively, for the anisotropic domelike dot which is truncated by the (114) and $(\bar{1}\bar{1}4)$ facets. Here, patterns for various sizes with the same dot shape are superposed to reduce the fringes due to the size effect; the base diameter d along $[1\bar{1}0]$ is varied from 12 to 20 nm while h/d is about 1/8 and w/d is about 5/8, where h is dot height and w is base length along [110]. Both patterns agree fairly well with the observed patterns. This indicates that the key point to reproduce the chevron spot is the curved surface of dot facing to $[1\bar{1}0]$ and $[\bar{1}10]$ azimuths.

The asymmetric intensity distribution in each of the simulated 113 and $\bar{1}\bar{1}3$ spots is, however, much more remarkable in Fig. 3(f) than the observed one. The asymmetry is also visible in Figs. 3(c) and 3(d). If the lateral expansion of the dots due to the strain relaxation is inhibited in the calculations, the simulated spot shapes become almost symmetric both for the domelike dot and for the {114}-truncated domelike dot. Therefore, the enhancement of the inner tail (short in reciprocal space) in the calculations is possibly related with the inhomogeneous increase (long in real space) of lateral atomic distances by the strain relaxation in the dot; in the region where the refraction shifts are substantial to form the tail, i.e., in the vicinity of the top of the dot, the lateral relaxation is also large. We expect that the spot shape asymmetry would be reduced by the multiple scatterings of the electrons among the 113, $\bar{1}\bar{1}3$, and other beams (mixing of different spot shapes), which are not included in the present calculations.

It must be noted that the asymmetry would be reduced to some extent also owing to the strain mediation brought about by the incorporation of Ga into the dots from the GaAs substrate.[18–20] Although, we ignored the cation interdiffusion for simplification, its effect on the refractions is not so serious because mean inner potentials of InAs and GaAs calculated from the atomic scattering factors are almost identical to be 15.3 eV; both the atomic scattering factor and volume of In are larger than those of Ga. Therefore, the main effect of the interdiffusion on the RHEED pattern is induced by the contraction of the dots, which causes upward shifts of the Bragg spots at the same glancing angle of the electron beam, slight outward shifts of the side spots such as 113 and $\bar{1}\bar{1}3$, and the reduction of the intensity asymmetry between their tails. These trends can be confirmed by comparing Figs. 3(g) and 3(h), which show calculated patterns for the anisotropic truncated domelike dots composed of $In_{0.5}Ga_{0.5}As$ and GaAs, respectively, with Fig. 3(f). Here, the size of the dot for Figs. 3(g) and 3(h) are fixed and the fringes due to the size effect appear; The base diameter along $[1\bar{1}0]$ is 16 nm, the base length along [110] is 10 nm, and the height is about 2 nm.

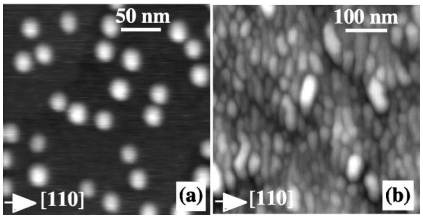

FIG. 5. AFM images of 1.7 ML InAs grown on GaAs(001) (a) and 4.4 ML InAs grown on InAlAs/InP(001) (b). The coverage of InAs includes the wetting layers.

The anisotropic truncated domelike dot also agrees with the observations of the InAs/GaAs(001) dots by scanning tunneling microscope (STM) in ultra high vacuum;[20,21] the dots are longer along $[1\bar{1}0]$ than along [110]. Figure 5 shows *ex situ* AFM images of the InAs/GaAs and InAs/InAlAs/InP dots. The anisotropy is not so obvious in Fig. 5(a) possibly and partly due to the tip convolution and oxidation effect on the small dots or difference on growth conditions such as III/V flux ratio. On the other hand, the InAs dots on InAlAs/InP(001) are larger because of lower lattice mismatch and clearly elongated along $[1\bar{1}0]$ as Fig. 5(b) in agreement with a previous report.[22] Furthermore, inhomogeneity in shape and size seems more pronounced. From these inhomogeneous dots, the chevron pattern is also observed as Fig. 1(d). Figures 3(i) and 3(j) show calculated RHEED patterns superposed with several elongated domelike (part of ellipsoid) dots whose base diameter along $[1\bar{1}0]$ d (16 to 29 nm) is two or three times larger than that along [110] and h/d is in the range from 0.024 to 0.053. Since the cross section of the elongated dome normal to the [110] azimuth is broad, the angle between the chevron tails is very small and the two tails overlap at [110] azimuth. Though the set of shapes and sizes of the dots was not optimized, the calculated patterns reproduce the anisotropy and the basic features in the observed patterns of Figs. 1(c) and 1(d) fairly well except for the disappearance of the 002 spot hiding below the shadow edge at $[1\bar{1}0]$ because of the large substrate-normal refractions at the relatively flat dot surfaces.

Finally, the {136}-facet dot, which was proposed in Ref. 6 and is also anisotropic, was examined as shown in Figs. 3(k)

and 3(l). The base length along $[1\bar{1}0]$ is 16 nm, which is two times larger than that along [110]. The electron beam is also refracted partly parallel to the substrate because the normal vector of the {136} facets is out of the incident plane like the path 2 and 3 in Fig. 4(a). In fact, the refraction effect parallel to the substrate is obvious at $[1\bar{1}0]$ incidence since the glancing angle to the facets at this azimuth is smaller than that at [110]. However, since the surface normal vector is fixed on a single facet, the extension of the tails due to refraction is limited in contrast with the domelike dots. If the top and the ridges along $[1\bar{1}0]$ of the {136}-facet dot are rounded to a certain extent, the tails presumably would be longer. Another possibility is a mixture of different shapes such as {136}, {125}, etc. In fact, {125}-facet dots were observed by STM.[21] In this case, the long tails are expected to be composed of various refraction shifts at different dots. However, the formations of the {125}-facet dots seems to be exceptional cases which depend on their local environments.[21]

We consider that the most probable models for the InAs dots which can reproduce the chevron tails of the $[1\bar{1}0]$ patterns are the ones which have curved surfaces facing $[1\bar{1}0]$ and $[\bar{1}10]$ azimuths. Moreover, the dot surfaces facing [110] and $[\bar{1}\bar{1}0]$ azimuths must be steeper than the former surfaces to suppress the refraction effect and to reproduce the oval spots of the [110] patterns. In this kind of models, the dot has more step kinks, which capture adatoms, on the former surfaces than on the latter surfaces. This implies that the dot grows more rapidly to $[1\bar{1}0]$ and $[\bar{1}10]$ directions and enhances the shape anisotropy further during growth. The narrow size distribution of the highly strained dots can be attributed to the strain-induced kinetic barrier at the dot edge (suppression of the growth after the nucleation).[23] The initial preferential formations of the straight terraces along $[1\bar{1}0]$ on the critical-size dots are, however, probably caused by the smaller free energies per area of the $(11n)$-oriented facets than those of the $(1\bar{1}n)$-oriented facets under the conventional III/V flux ratio.

The shapes of the self-assembled InAs nanostructures grown on the lower misfit InAlAs, InGaAs, and InP substrates strongly depend on the morphology[22] and growth method[24] of the buffer layers and sometimes become wire-like structures though the lattice misfits to InAs are the same. As shown in Fig. 5(b), the InAs dots on InAlAs are large and almost fully cover the surface because of the relatively small influence of the strain energy upon dot size and shape compared with the surface energy. Consequently, most of the deposited atoms fall on the islands and diffuse on the anisotropic terraces elongated along $[1\bar{1}0]$ and captured at the $[1\bar{1}0]$ or $[\bar{1}10]$ ends. Thus, it is suggested that the shapes of the InAs nanostructures on substrates with smaller lattice mismatch are more strongly controlled by the kinetics.

IV. CONCLUSIONS

It was demonstrated that the refractions of electron beam at the curved surface of dot can reproduce the chevron spot. We examined anisotropic InAs dots which have (i) domelike surfaces at the $[1\bar{1}0]$ and $[\bar{1}10]$ azimuths and facets facing the [110] and $[\bar{1}\bar{1}0]$ azimuths and (ii) domelike surface elongated along $[1\bar{1}0]$. Kinematically calculated RHEED patterns for these models agree fairly well with observations at both [110] and $[1\bar{1}0]$ azimuths. These results pointed out the importance of the refraction effect in the analysis of electron diffraction from certain kind of nanostructures.

ACKNOWLEDGMENTS

One of the authors (T.H.) acknowledges support from Nippon Sheet Glass Foundation for Materials Science and Engineering.

[1] W. Yang, H. Lee, T.J. Johnson, P.C. Sercel, and A.G. Norman, Phys. Rev. B **61**, 2784 (2000).
[2] L.W. Wang, J. Kim, and A. Zunger, Phys. Rev. B **59**, 5678 (1999).
[3] O. Stier, M. Grundmann, and D. Bimberg, Phys. Rev. B **59**, 5688 (1999).
[4] Y. Nabetani, T. Ishikawa, S. Noda, and A. Sasaki, J. Appl. Phys. **76**, 347 (1994).
[5] H. Yamaguchi, M.R. Fahy, and B.A. Joyce, Appl. Phys. Lett. **69**, 776 (1996).
[6] H. Lee, R. Lowe-Webb, W. Yang, and P.C. Sercel, Appl. Phys. Lett. **72**, 812 (1998).
[7] H. Saito, K. Nishi, and S. Sugou, Appl. Phys. Lett. **74**, 1224 (1999).
[8] G. Hollinger, M. Gendry, J.L. Duvault, C. Santinelli, P. Ferret, C. Miossi, and M. Pitaval, Appl. Surf. Sci. **56-58**, 665 (1992).
[9] T. Hanada, H. Totsuka, and T. Yao, Jpn. J. Appl. Phys., Part 1 **40**, 1878 (2001).
[10] B.H. Koo, T. Hanada, H. Makino, J.H. Chang, and T. Yao, J. Cryst. Growth **229**, 142 (2001).
[11] F.H. Stillinger and T.A. Weber, Phys. Rev. B **31**, 5262 (1985).
[12] M. Ichimura, Phys. Status Solidi A **153**, 431 (1996).
[13] C. Pryor, J. Kim, L.W. Wang, A.J. Williamson, and A. Zunger, J. Appl. Phys. **83**, 2548 (1998).
[14] P.A. Doyle and P.S. Turner, Acta Crystallogr., Sect. A: Cryst. Phys., Diffr., Theor. Gen. Crystallogr. **A24**, 390 (1968).
[15] The calculated facet is slightly (about 2 to 3°) steeper than the ideal bulk-truncated facet owing to substrate-parallel compressive strain and substrate-normal tensile strain in a strain-induced dislocation-free dot.
[16] J.F. Menadue, Acta Crystallogr., Sect. A: Cryst. Phys., Diffr., Theor. Gen. Crystallogr. **A28**, 1 (1972).
[17] After the submission of the present paper, we noticed that a paper had been published [D.W. Pashley, J.H. Neave, and B.A. Joyce, Surf. Sci. **476**, 35 (2001)] on the same subject which draws identical conclusions, but based on a somewhat different approach.
[18] P.B. Joyce, T.J. Krzyzewski, G.R. Bell, B.A. Joyce, and T.S.

Jones, Phys. Rev. B **58**, R15 981 (1998).
[19] I. Kegel, T.H. Metzger, A. Lorke, J. Peisl, J. Stangl, G. Bauer, J.M. García, and P.M. Petroff, Phys. Rev. Lett. **85**, 1694 (2000).
[20] B.A. Joyce, T.S. Jones, and J.G. Belk, J. Vac. Sci. Technol. B **16**, 2373 (1998).
[21] Y. Hasegawa, H. Kiyama, Q.K. Xue, and T. Sakurai, Appl. Phys. Lett. **72**, 2265 (1998).
[22] J. Brault, M. Gendry, G. Grenet, G. Hollinger, Y. Desières, and T. Benyattou, Appl. Phys. Lett. **73**, 2932 (1998).
[23] A.-L. Barabási, Appl. Phys. Lett. **70**, 2565 (1997).
[24] L. González, J.M. García, R. García, F. Briones, J. Martínez-Paster, and C. Ballesteros, Appl. Phys. Lett. **76**, 1104 (2000).